

Development of a Pedestrian Pelvis Impactor CAE Model with Potential to Address Pelvis Injury Loads and Injury Mechanisms

Takahiro Isshiki, Yu-ki Higuchi, Ryouyusuke Kato, Jacobo Antona-Makoshi, Atsuhiko Konosu, Yukou Takahashi

Abstract This study aimed to clarify the feasibility to develop a biofidelic Pedestrian Pelvis Impactor (PPI) CAE model with the potential to address detailed pelvic loading and injury mechanisms. First, three simplified car front-end models (Sedan, SUV with a low/high bonnet leading edge) were applied to simulate impacts at different locations along the thigh of a biofidelic 50th percentile male human body model (HBM). Based on these simulations, the loads and the stresses sustained by the pelvis were analysed, and the pelvic ring and the ilium on the struck side were identified as the minimum structural elements required to represent the pelvic loading condition adequately. Based on the analysis, a PPI CAE model that incorporated the assumed structural simplifications was developed. In order to enable a biofidelity evaluation of the PPI model, the model was complemented with the lower limb and the pelvis flesh at the struck side from the HBM. Both the complemented PPI model and the complete HBM were subjected to a variety of simulated impacts with 36 simplified car front-end models (18 Sedan and 18 SUVs). The PPI model response highly correlated with the HBM response in terms of peak pelvis injury measures except for sacroiliac force .

Keywords Impactor pedestrian safety, pelvis injury.

I. INTRODUCTION

The lower limbs and the head are the most frequently injured body regions in a car-to-pedestrian accidents worldwide [1]. The global technical regulation for pedestrian safety [2] and the United Nations regulation for pedestrian safety [3] were developed to reduce such injuries at the global level. Recent accident data from Japan shows that, along with these two body regions, pelvic injuries are also relatively frequent. More precisely, in the year 2016, the ratios of main injured body regions in accidents involving serious and fatally injured pedestrians were 32%, 25% and 13% for the lower limbs, the head and the pelvis, respectively [4]. In addition, car to pedestrian accident data analysis in the US has shown that SUVs can cause more serious-to-fatal pelvic injuries compared to Sedans [5]. This calls for enhanced pelvic protection for pedestrians.

One common approach for the prevention of pedestrian injuries is the evaluation of the safety performance of car front-ends through standardised impact tests using pedestrian impactors that mimic the body regions to be protected. Such tests have been specified by global regulations (UN GTR No.9 and UN R No.127) and New Car Assessment Programmes. In the 1990s, the European Enhanced Vehicle-Safety Committee (EEVC) developed a pedestrian upper legform impactor to evaluate pelvis and femur injury probability in a car-to-pedestrian impacts [6]. However, the EEVC impactor mimics the central part of the thigh of a pedestrian, and therefore, it cannot appropriately address the loads and kinematics sustained by the pelvis in a car-to-pedestrian impacts [7]. A previous study investigated the influence of the upper body and the lower limb of a pedestrian on a pelvic injury measure (pelvis deflection) [8]. However, the previous study did not analyse the loads sustained by the pelvis or pelvic injury mechanisms.

The ultimate long term goal of this research is to contribute to the reduction of pelvic injuries sustained by pedestrians when hit by the frontal part of a car. The specific aim of this study is to develop a biofidelic PPI CAE Model with the potential to represent pelvis injury mechanisms in a car-to-pedestrian impacts, and to evaluate the model's biofidelity under various car impact conditions.

II. METHODS

A two-step approach was applied in this study. The first step aimed to investigate the pelvis structural

Takahiro Isshiki (phone: +81-29-856-0885, e-mail: tissiki@jari.or.jp), Yu-ki Higuchi, Ryouyusuke Kato, Jacobo Antona-Makoshi, and Atsuhiko Konosu are researchers at the Japan Automobile Research Institute, Tsukuba, Japan. Yukou Takahashi is the chairperson of the Pedestrian Safety Experts Group at the Japan Automobile Manufacturers Association, Inc., Tokyo, Japan.

elements required to mimic pelvis injury mechanisms in car to pedestrian impacts. With this purpose, the loads sustained by the pelvis were analysed using a 50th percentile male human body model (HBM), and three simplified car models (SCMs). The biofidelity of the HBM, including the pelvis, was validated in detail in previous work at the component and the full-body levels [5][7][9]. The SCMs represented the front-end of a sedan (Sedan), a SUV with a low bonnet leading edge (SUV-Low SCM) and an SUV with high bonnet leading edge (SUV-High SCM).

In the second step, a PPI CAE model was developed based on the results from the first step. The biofidelity of this model was evaluated under a variety of impact conditions with 36 SCMs (18 low and 18 high bumper) [10-13] by conducting linear correlation analysis between the peak pelvic injury measures from the the PPI CAE model and those from the HBM.

Step 1: Analysis of Pelvis Injury Mechanisms and Applied Loads onto the Pelvis

Three car-to-pedestrian impacts at 40 km/h were simulated using each of the three SCMs and the HBM as shown in Fig.1. The SCMs geometrical specifications were selected to ensure different impact conditions along the lower extremity of the HBM. The Sedan SCM impacted the pedestrian model at the middle of the thigh and below. The SUV-Low SCM impacted the upper thigh region and below. The SUV-High SCM impacted the pelvis area and below. The geometrical and structural specifications of the SCMs were based on commercial vehicle data of sedans and SUVs and have been used in previous work [10-13]. Detailed specifications of the SCMs applied in the current study are shown in Appendix A. The SCMs were set to impact the HBM laterally to the impacted lower limb in a straight and vertical posture and with the sole of the foot 25 mm above the ground, as specified in UN regulations (GTR No.9 and UN R No.127). A friction coefficient of 0.4 was applied to the HBM and the ground contact, and 0.3 to the HBM and the SCMs. Gravity field (9.8 m/s²) was applied to the whole model.

Impact speed: 40 km/h

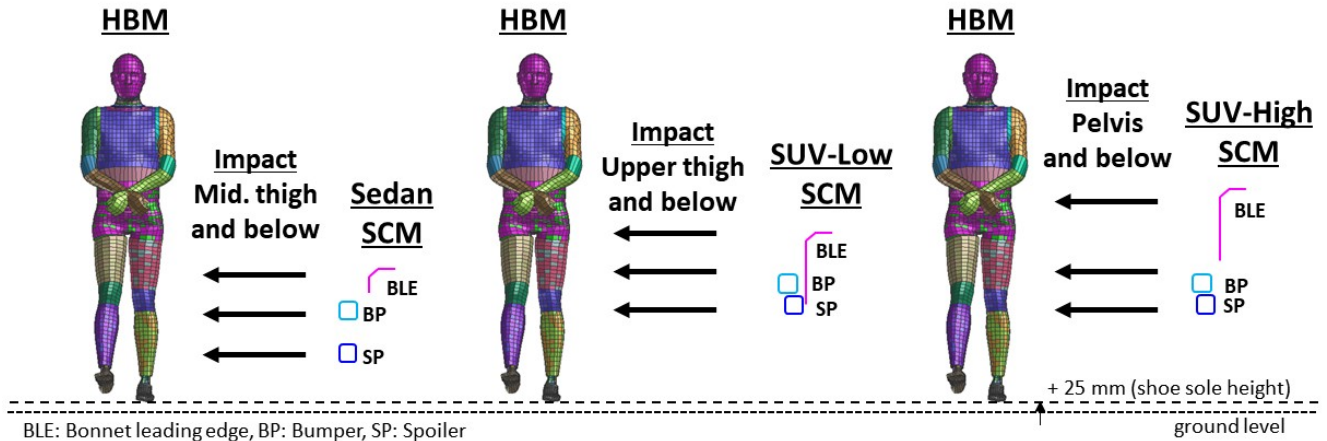


Fig. 1. Three different SCMs (Sedan SCM, SUV-Low SCM, SUV-High SCM) and HBM impact conditions.

Based on the three simulations, HBM kinematics and external loads sustained during the impacts, pelvis internal loads, as well as injury measures and local stresses sustained by the pelvis were examined to understand possible pelvis injury mechanisms. Pelvis deflection [14] and pubic force [15] were selected as injury criteria for pubic rami fractures (Fig. 2), which tend to occur frequently in car-pedestrian accidents [16-17]. In addition, sacroiliac joint force [15] was also selected as an injury criterion for sacroiliac joint fractures which occur less frequently, but can be devastating [17].

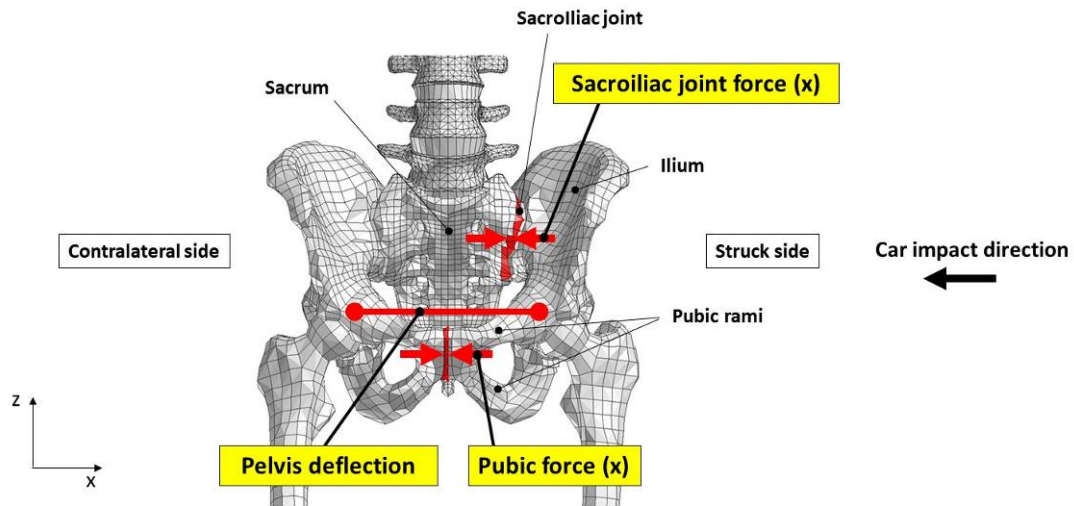


Fig. 2. Pelvic injury criteria applied in the current study (pelvis deflection, pubic force and sacroiliac joint force).

Fig. 3 illustrates a schematic of the forces applied to the pelvis during a car-to-pedestrian impact. First, from the struck side, two major forces are applied in the car impact direction: the ilium force (F-a1) and the acetabulum force (F-a2). These forces are generated by the car impacting the ilium (via the flesh around the hip) and the lower limb, respectively. Second, from the contralateral side, two major inertial forces are applied to the pelvis: the contralateral side hip flesh inertial force (F-b1) and the contralateral side lower limb inertial force (F-b2). These forces are generated by the acceleration of the flesh and the lower limb against the car impact, respectively. Finally, inertial force of the upper body (F-c) applied to the upper part of the pelvis is generated by the translation/rotation of the upper body towards the impacting car. Those forces were investigated to evaluate which forces are essential to represent pelvic loading condition in a car impact scenario to develop an impactor by simplification of pelvic structure.

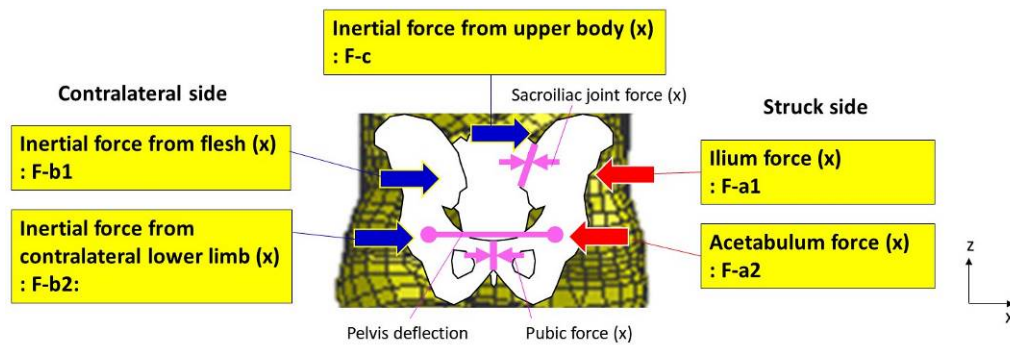


Fig. 3. Schematic of the applied pelvic loads and the related injury measures.

Step 2: Development and Validation of the PPI CAE model

A PPI CAE model was developed based on the results from the Step 1. The pelvis consisted of a largely simplified pelvic-like geometry, based on the assumption that a precise shape of the HBM is not necessary to evaluate pelvis injury. The HBM parts that were found unnecessary for pelvis injury evaluation, were simply not incorporated to the PPI model design. The HBM parts which inertial effects were considered necessary for pelvis injury evaluation were incorporated into the PPI model design in the form of effective masses attached to their main working point. The effective mass for each HBM impact simulated with the 36 SCMs was calculated using the inertial forces and accelerations generated on the main working point at the HBM. The effective mass applied to all the simulations with the PPI model was defined by averaging the effective masses calculated from the HBM simulations (Appendix B and C). Material properties in the PPI model were kept the same as the HBM, so in the current study the main focus was on simplified structure and geometry.

For PPI CAE model biofidelity evaluation purpose, the model was combined to the human lower limb and the flesh around the hip from the struck side of the HBM, as these parts were essential to represent

car-to-pedestrian impact conditions according to the findings in Step 1. The attachment between the lower limb from the human model and the PPI CAE model was done via a free spherical joint, by assuming that human hip joints have low resistance to rotation. The combined model was named as PPI CAE model evaluation model (PPI-EM).

The validity of the developed PPI CAE model was evaluated by comparing the PPI-EM response with that of the HBM at impacts with 36 SCMs, 18 of them representing low bumper cars and 18 high bumper cars (Fig. 4). Peak pelvic injury measures were extracted from the simulations with the PPI CAE model and the HBM, and correlation analysis between the extracted measurements was conducted. Preliminary acceptable range of coefficient of determination (R^2) of 0.5 and higher, and of regression coefficient (slope) between 0.8 to 1.2 were set as targets that would represent similar or better performance than other existing pedestrian impactors [10-13, 17].

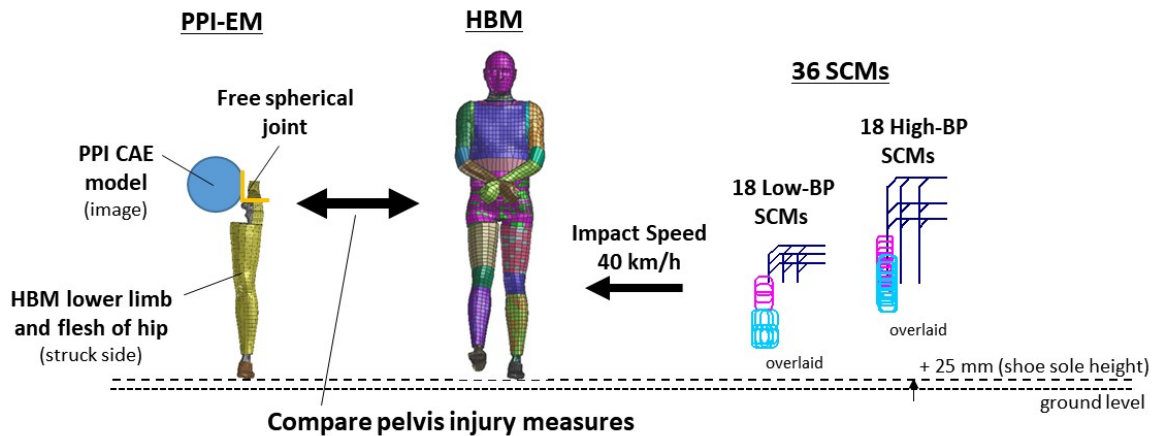


Fig. 4. Validation method.

III. RESULTS

Step 1: Analysis of Pelvis Injury Mechanisms and Applied Loads onto the Pelvis

HBM External Loading Conditions. Fig. 5 to Fig. 7 show sequential images of the overall HBM impact kinematics and contact forces between the car front-end and three sections along the struck side of the HBM (hip, thigh and leg) in impacts with the three different SCMs.

In the impact with the Sedan SCM, the vehicle contact initiates in the leg and spreads up to the thigh region, causing maximum contact forces of around 6 kN and 3 kN, respectively (Fig. 5).

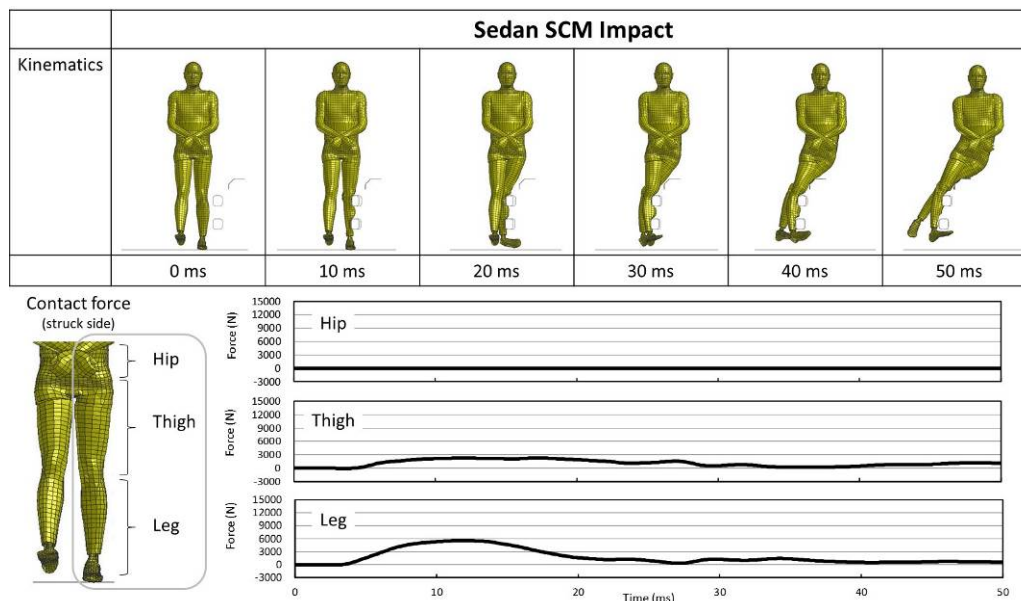


Fig. 5. Kinematics and applied loads onto the HBM at impact with Sedan SCM.

In the impact with the SUV-Low SCM, the impact energy is transferred almost exclusively to the thigh region causing maximum thigh contact forces of around 9 kN in that region (Fig. 6). In the impact with the SUV-High SCM, the contact between SCM and the HBM initiates at the thigh and is followed by a raise in the hip area due to direct contact between the bonnet leading edge and the flesh surrounding the pelvis/ilium area. This impact causes the highest hip and thigh loads among the three SCMs with peaks around 9 and 12 kN, respectively (Fig. 7).

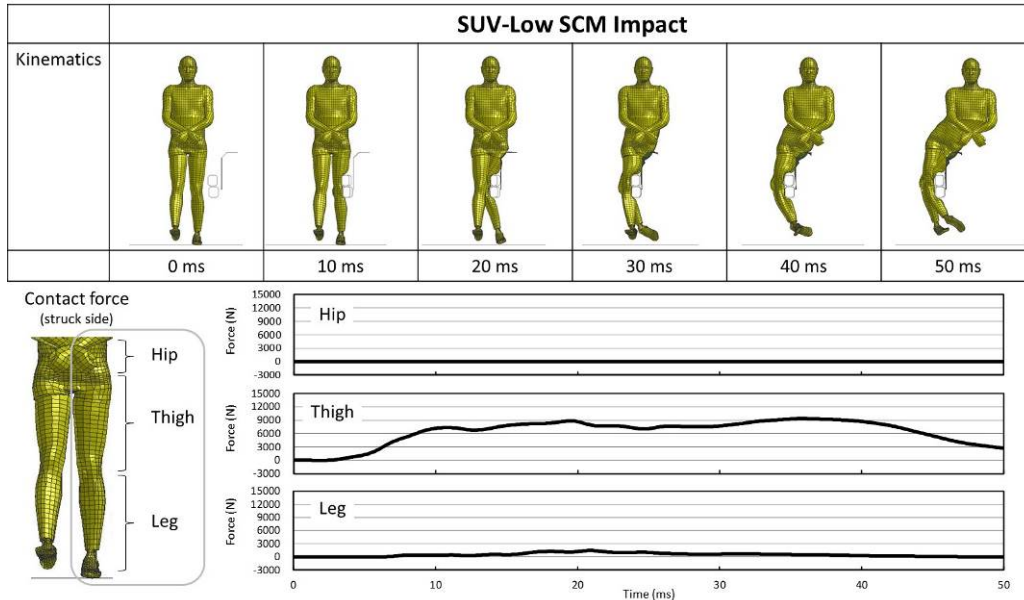


Fig. 6. Kinematics and applied loads onto the HBM at impact with SUV-Low SCM.

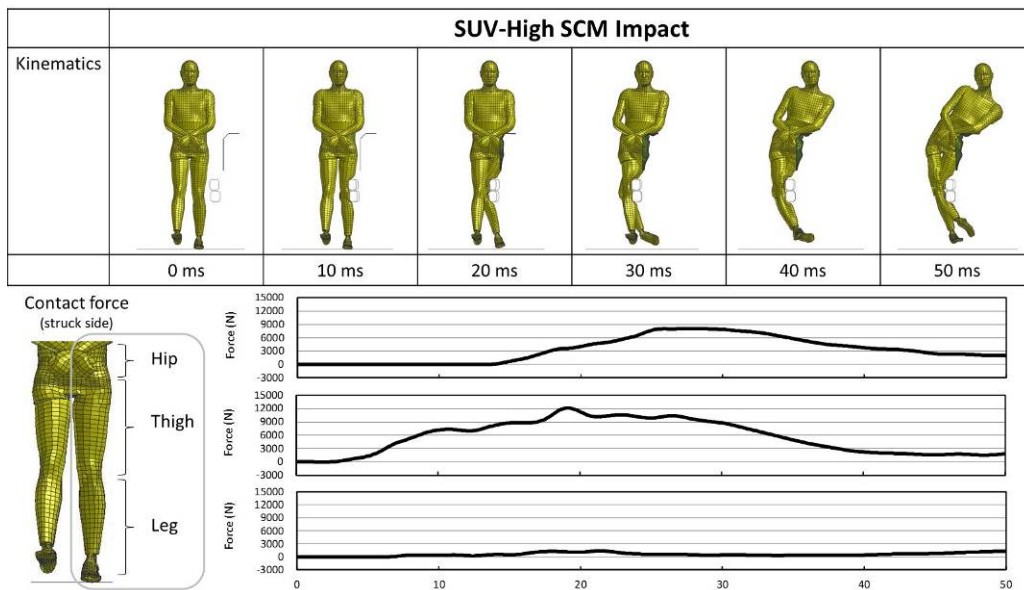


Fig. 7. Kinematics and applied load onto the HBM at impact with SUV-High SCM.

Pelvis Internal Loading Conditions: Fig. 8 to Fig. 10 show pelvic internal forces time histories in impacts with the three SCMs. Similarly, Fig. 11 and Fig.12 show pelvic injury measures, and pelvic equivalent stresses for the same impacts, respectively.

In the impact with the Sedan SCM, only F-a2 was observed on the struck side, because no contact between the car front-end and the ilium occurred. In addition, the contact between the SCM and the HBM occurred at the middle of the thigh and below, which caused rotation of the hip joint and a reduction of the compressive load induced to the pelvis via hip joint. Therefore, the applied pelvic forces were low (around 1 kN), which implies low pelvic injury measures (Fig. 11, left column) and corresponding pelvic stresses (Fig. 12, upper row).

In the impact with the SUV-Low SCM, the SCM impacted the upper part of the thigh in the vicinity of the pelvis. This induced high acetabulum forces (F-a2 of 6 kN) and high inertial forces from the contralateral impact side (F-b1 and F-b2 are approximately 2 kN, respectively). This caused increased injury measures and equivalent stresses at the pelvis, compared to those with the Sedan SCM impact. For the SUV-Low SCM impact, the F-c value is still low (around 0.5 kN) at the time by which all peak pelvic injury measures have reached their peak.

In the impact with the SUV-High SCM, F-a1 and F-a2 were high because the SCM impacted the ilium via the flesh as well as the upper part of the thigh directly. Both forces are over 5 kN, which causes the highest pelvis acceleration, contralateral inertial force (F-b1 and F-b2 are approximately 4 kN, respectively), injury measures and equivalent stresses among the three SCMs.

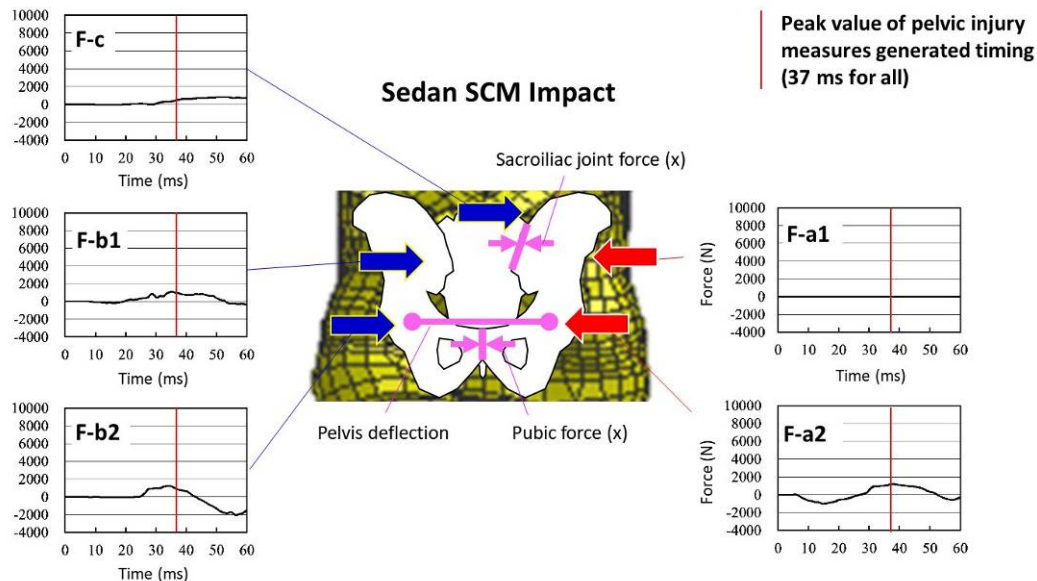


Fig. 8. Applied loads at the pelvis in impact with the Sedan SCM.

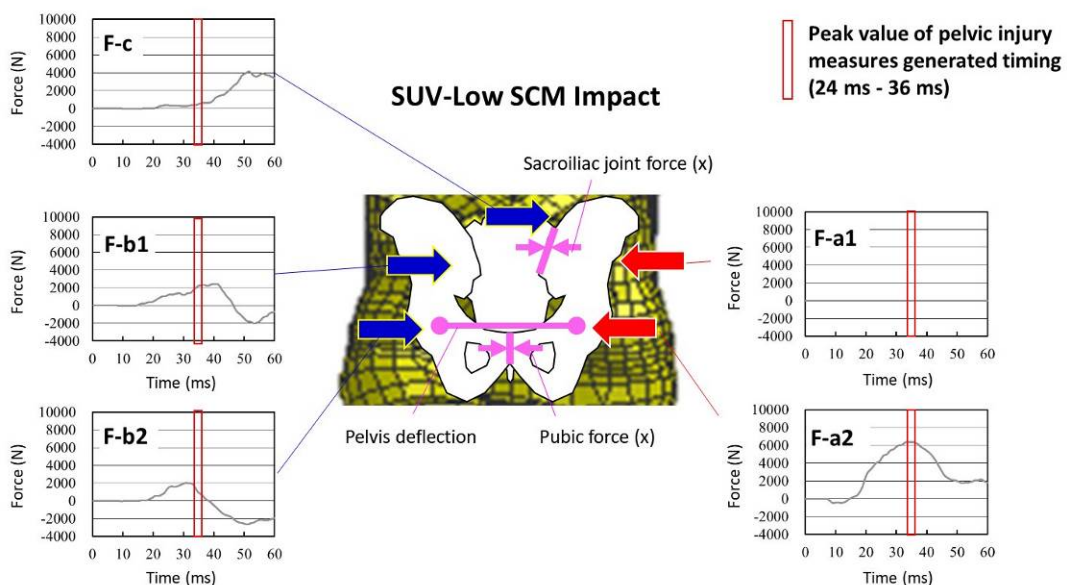


Fig. 9. Applied loads at the pelvis in impact with the SUV-Low SCM.

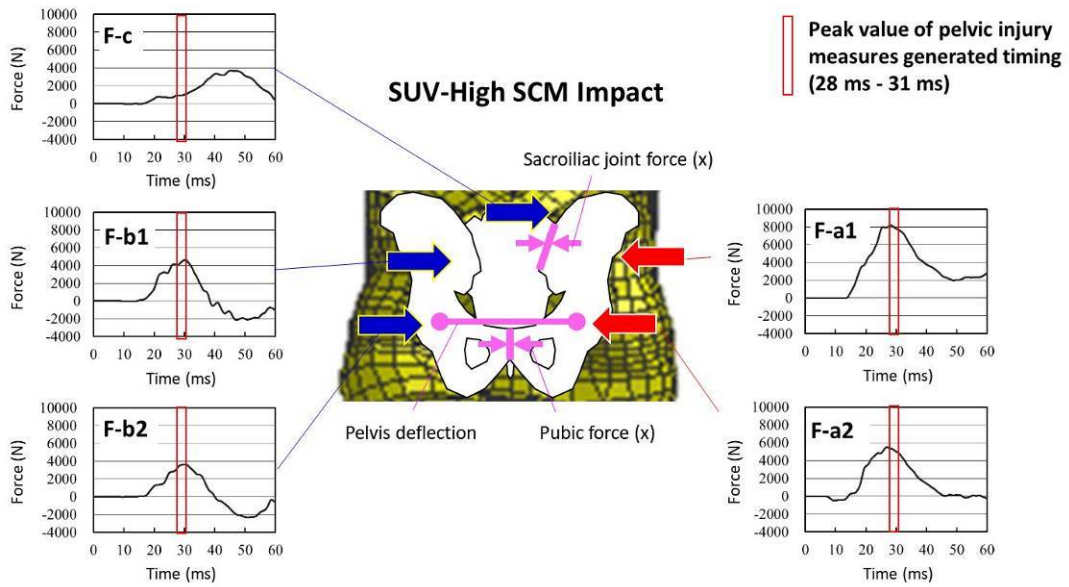


Fig. 10. Applied loads at the pelvis in impact with the SUV-High SCM.

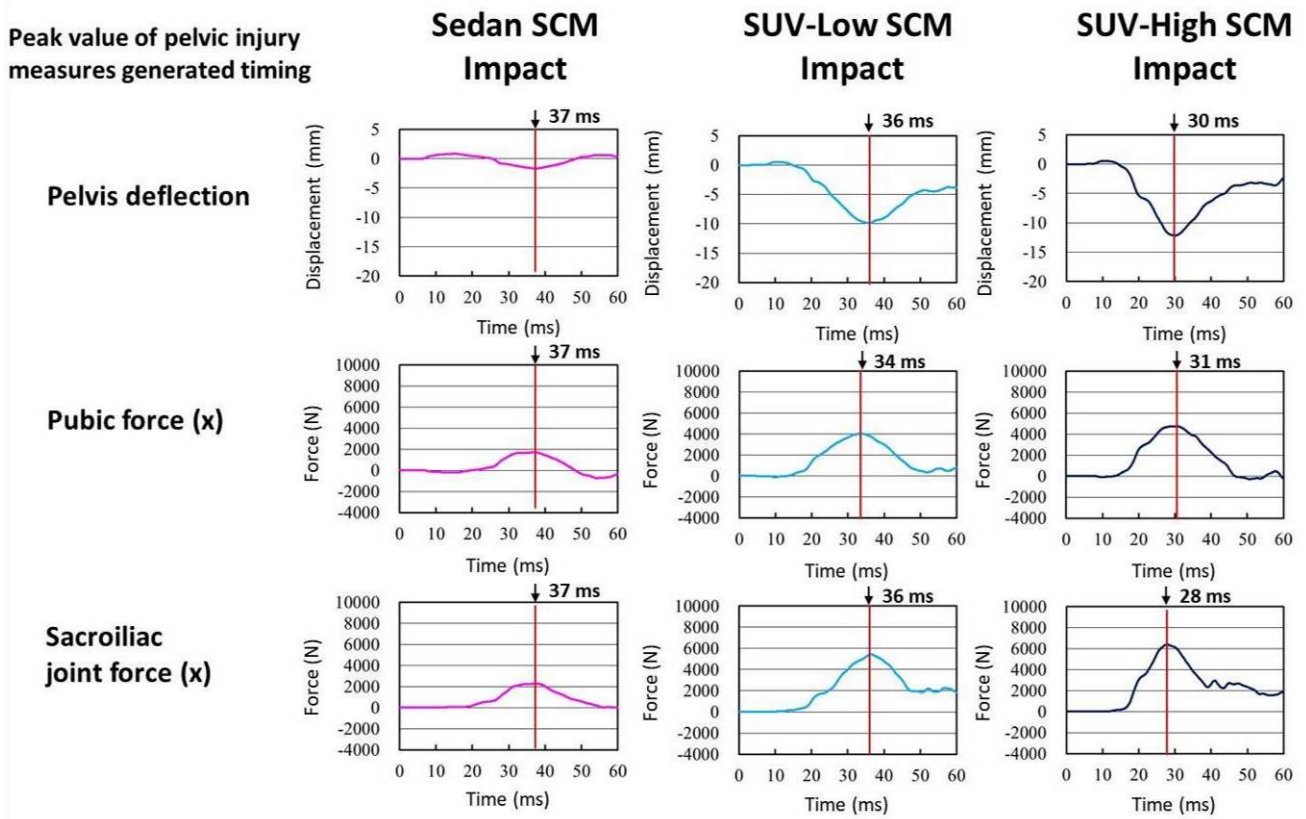


Fig. 11. Pelvis injury measures waveforms in impact with three SCMs.

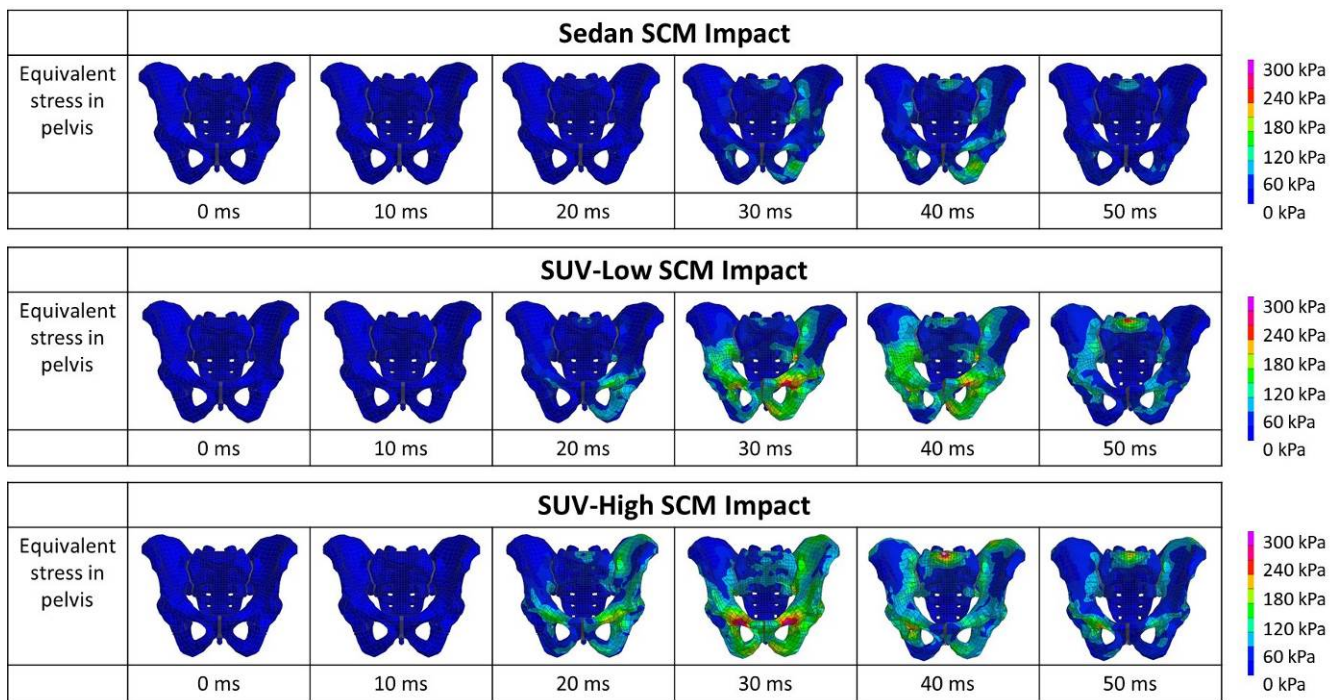


Fig. 12. Equivalent stress at the pelvis in impact with three SCMs.

Relevant Component Selection

Based on the results in Step 1, it was determined that the lower limb and the flesh of the hip on the struck side are essential to represent the external energy transfer mechanisms between the car front-end components and the lower extremity, which defines the pelvis internal loading conditions. With regards to the pelvis internal loading conditions, it was presumed that ilium and acetabulum forces on the struck side (F-a1 and F-a2 in Fig.8 to Fig.10), as well as the inertial forces induced by the flesh and the contralateral lower limb (F-b1 and F-b2 in Fig.8 to 10) are essential to evaluate pelvis injury measures, but the inertial force induced by the upper body (F-c in Fig.8 to 10) is not. With regard to the necessary pelvis structural components, it was determined that the pelvic ring and the ilium on the struck side are essential to capture the high stresses observed in impacts with the SUV-High SCM (Fig. 12, bottom row). Other pelvis parts sustained low stresses, and therefore those parts may be largely simplified and still allow for the evaluation of the key pelvis injury mechanisms.

Step 2: Development of the PPI CAE Model and Validation

Based on the results from Step 1, the PPI CAE model shown in Fig.13 was developed. The PPI model consists of a highly simplified symmetric pelvic ring with an ilium component on the struck side and two effective masses added to the ilium on the contralateral side (3.43 kg) and to the location of acetabulum of HBM on the contralateral side (3.87 kg), respectively. The former mass was incorporated into the PPI model by increasing the density of the contralateral ilium. This was done to attempt to compensate for the overall inertial force that the flesh on the contralateral side exerts on the contralateral ilium. The latter mass was applied to a single node positioned at the location corresponding to the center of rotation of the hip. The node was then rigidly connected to the nodes in the area corresponding to the acetabulum. This was done to compensate for the inertial force that the contralateral lower limb exerts on the pelvis via the hip joint. The detailed process applied to calculate these masses is presented in Appendix B and C.

In order to evaluate the biofidelity of the PPI CAE model by comparison with the HBM, a specific model that combined the PPI CAE previously described (Fig. 13) with the hip flesh and the lower limb from the struck side of the HBM was developed. The PPI CAE model was attached to the lower limb through a free spherical joint (Fig. 14) based on assumed low resistance to rotation. In this study, the PPI CAE model was not combined with an existing legform impactor model to exclude the influence of any limitations of biofidelity of the legform impactor model. The PPI CAE model with the human lower limb and hip flesh models was denoted as PPI evaluation model (PPI-EM).

Fig. 15 shows linear correlation results between the injury measures using the PPI-EM and those from the full HBM in impacts with the 36 SCMs. Correlation coefficients between the peak pelvic injury measures from the PPI CAE model and those from the HBM of 0.944, 0.875 and 0.613 for pelvis deflection, pubic force sacroiliac joint force, respectively were obtained which fell within the preliminary acceptable range values target of 0.5 and higher. On the other hand, relatively low values for the slope of the regression were obtained (pelvis deflection: 0.705, pubic force: 0.801, sacroiliac joint force: 0.744), which fell below the targeted range between 0.8 to 1.2 for pelvis deflection and sacroiliac joint force. Moreover, the peak sacroiliac joint force of the PPI CAE model deviated largely from the regression line between the PPI-EM and the HBM in two SUV impacts (SUV06 and SUV15 in Fig. 15).

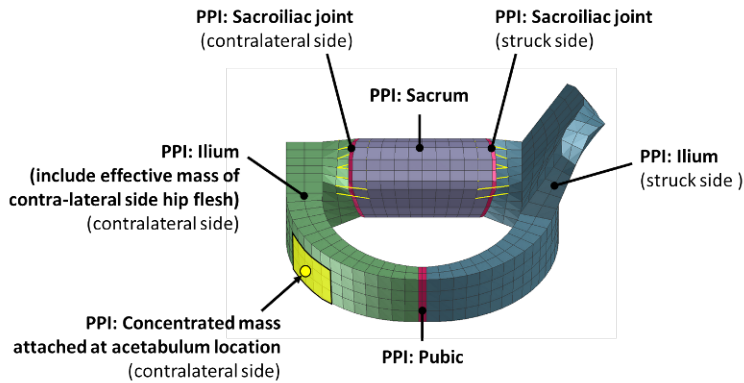


Fig.13. General construction of the PPI CAE model.

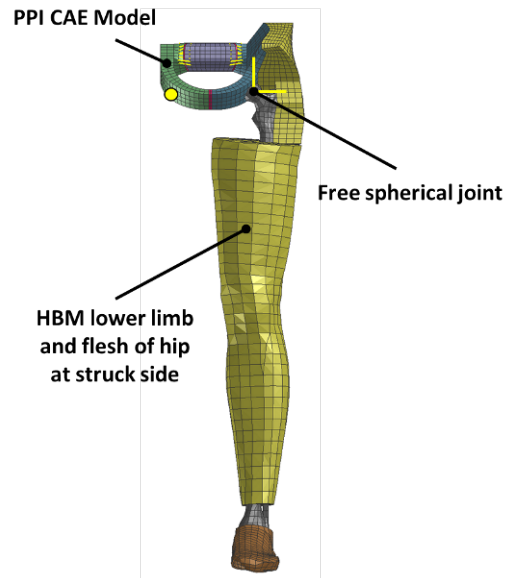


Fig.14. General construction of the PPI evaluation model (PPI-EM).

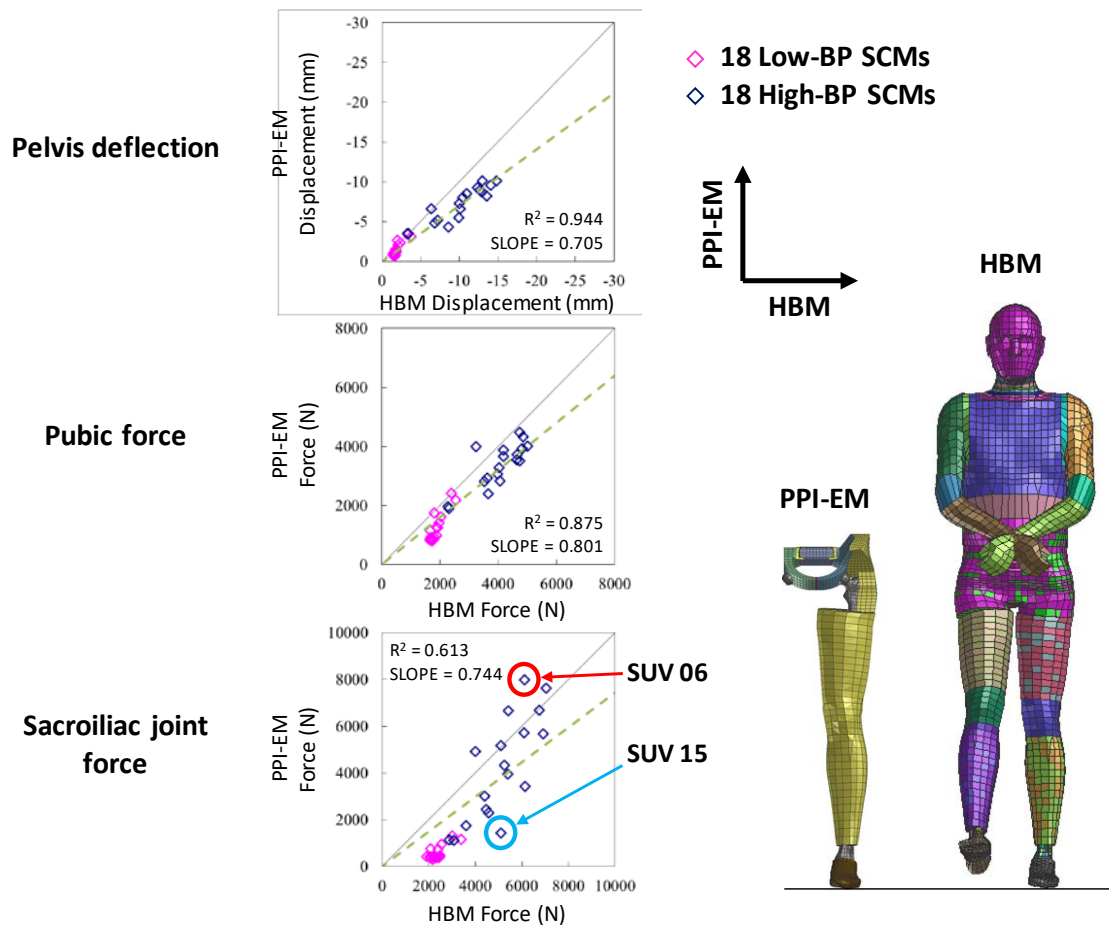


Fig.15. Results of correlation analysis for pelvis injury measures between the PPI CAE Model of PPI-EM and the pelvis of HBM.

IV. DISCUSSION

In this study, a PPI CAE model has been developed based on a preliminary evaluation of the pelvis internal loading mechanisms and possibly associated pelvis injury mechanisms. The proposed PPI model design has a largely simplified and asymmetric structure in opposition to that of the HBM. Despite the simplifications, the PPI model peak injury measures highly correlated with those from the HBM (pelvis deflection: $R^2 = 0.944$, pubic force: $R^2 = 0.875$, sacroiliac joint force: $R^2 = 0.61$) under a wide range of vehicle front-end designs, represented by 36 SCMs. The high correlations show the potential the PPI model can represent internal loads in the pelvis in a car-to-pedestrian impact. Nevertheless, differences between the PPI CAE model and the pelvis of HBM were also observed, which caused low slope values for the regression lines for pelvis deflection (0.705) and sacroiliac joint force (0.744), below the targeted range (0.8-1.2). This difference may be related to the differences in pelvis kinematics between the PPI model and the HBM.

Three-dimensional pelvis kinematics needs to be accounted for in order to increase the pelvic impactor's biofidelity. The peak sacroiliac joint force of the PPI CAE model deviated largely from the regression line between the PPI-EM and the HBM in two SUV impacts (SUV06 and SUV15 in Fig. 15). In both cases, the z-axis rotational kinematics between the PPI CAE model and the Pelvis of the HBM differed (Fig. 16). In the impact with the SUV 06, the pelvis was engaged, and the PPI CAE model showed smaller pelvis z-axis rotation than the HBM. This generated higher sacroiliac joint forces for the PPI-EM, due to the higher compressive pelvic forces sustained by the PPI CAE model. In the impact with the SUV 15, the pelvis was not engaged and the PPI CAE model showed larger z-axis rotation than the HBM. This generated lower sacroiliac joint forces in the PPI CAE model, due to lower compressive forces generated by increased PPI CAE model z-axis rotation.

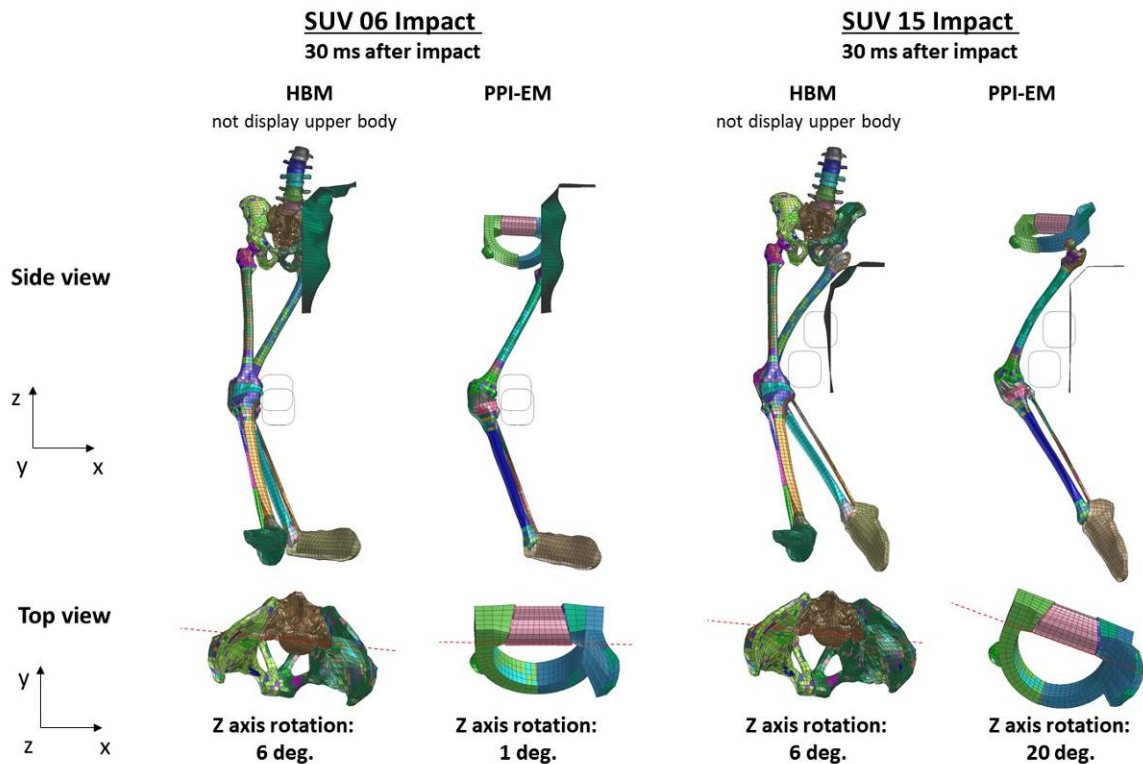


Fig.16. Kinematics of the PPI-EI and the HBM at impact with SUV 06 and SUV 15 (after 30 ms at impact).

The differences observed in pelvis kinematics between the PPI model developed and the HBM may be associated with the assumptions adopted to simplify the impactor's design. For example, the upper body was not incorporated into the PPI model because its influence on the pelvis lateral compressive forces was relatively low. Another example is the substitution of the contralateral lower limb by an effective mass at the hip joint as an attempt to mimic the inertial effect of the limb on pelvic lateral compressive forces. None of these simplifications considered the effect that the upper body or the contralateral limb may exert on vertical pelvis rotation. Therefore, further investigations on the effect of the simplifications applied to the three-dimensional kinematics of the pelvis are required. In addition, several issues in relation to the effective mass applied in this study require further clarifications. First, the mass was obtained from force and acceleration averaged over the time interval from the impact to the latest timing of all peak injury measures. Second, the effective mass varies for different SCMs (Appendix B and C) and an average value was adopted in the model. The above issues may also affect the three-dimensional kinematics of the PPI model and need to be addressed in future work.

In addition to the three-dimensional kinematics of the PPI CAE model, geometric simplifications adopted to develop the PPI CAE model may also affect the model's biofidelity. An example of this is the simplified geometry of the sacroiliac joint, which may have affected the sensitivity of the sacroiliac joint force measured by the PPI model in comparison with the HBM.

In summary, in order to enhance the biofidelity of the PPI CAE model, further analysis of the geometrical simplifications adopted, incorporation of construction materials and evaluation of the methodology to obtain the effective masses in considerations of three-dimensional pelvis kinematics, and optimisation of its components are needed.

V. LIMITATIONS

The PPI CAE model was evaluated through impacts with SCMs that mimic the central part of the car front-end structure. No angled bumper/spoiler/bonnet leading edge parts were considered, and therefore, additional validation including non-central parts of car front structures may be required. In addition, it is uncertain if the current mechanical PPI is compatible with existing mechanical lower limb impactors. The compatibility of the current pelvis impactor design proposed with existing mechanical lower limb from the

advanced Pedestrian Legform Impact (aPLI) [10-13] will also be investigated in the future.

VI. CONCLUSIONS

In this study, a novel PPI CAE model has been developed. The model considers detailed pelvis injury loads and corresponding injury mechanisms in a wide range of simulated car-to-pedestrian impacts. Despite a largely simplified structure compared to that of a HBM, the PPI model response highly correlated with the HBM in terms of pelvis deflection and pubic force, whereas only moderately in terms of sacroiliac forces. The current study warrants further research to enhance the biofidelity of the PPI CAE model presented.

VII. REFERENCES

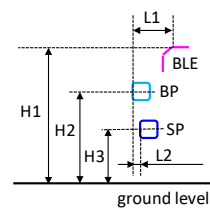
- [1] Mizuno Y. Summary of IHRA pedestrian safety WG activities (2005) proposed test methods to evaluate pedestrian protection afforded by passenger cars. *Proceedings of 19th ESV Conference, 2005, Washington DC, USA.*
- [2] United Nation. UN Global Technical Regulation (GTR) No.9 (Pedestrian Safety).
- [3] United Nation. UN Regulation (R) No. 127 - Rev.2 – Pedestrian Safety.
- [4] ITARDA. "Statistics of traffic accident data in Japan, in Japanese, 2016" Internet: [<http://www.itarda.or.jp/materials/publications.php?page=4>], 17 July 2018 [31 March 2019].
- [5] Kikuchi Y, Takahashi Y, and Mori F. Full-scale validation of a human FE model for the pelvis and lower limb of a pedestrian. *SAE Technical Paper, 2008, 01-1243.*
- [6] EEVC. EEVC working group 17 report - improved test methods to evaluate pedestrian protection afforded by passenger cars (December 1998 with September 2002 updates).
- [7] Takahashi Y, Suzuki S, Ikeda M and Gunji Y. Investigation on pedestrian pelvis loading mechanisms using finite element simulations. *Proceedings of IRCOBI Conference, 2010, Hanover, Germany.*
- [8] Gunji Y., Okamoto M. and Takahashi Y. Examination of human body mass influence on pedestrian pelvis injury prediction using a human FE model. *Proceedings of IRCOBI Conference, 2012, Dublin, Ireland*
- [9] Kikuchi Y, Takahashi Y, and Mori F. Development of a finite element model for a pedestrian pelvis and lower limb. *SAE Technical Paper, 2006, 01-0683.*
- [10] Isshiki T, Konosu A, and Takahashi Y. Development and evaluation of the advanced pedestrian legform impactor prototype which can be applicable to all types of vehicles regardless of bumper height - Part 1: finite element model. *Proceedings of IRCOBI Conference, 2016, Malaga, Spain.*
- [11] Isshiki T, Antona-Makoshi J, Atsuhiko K, and Takahashi Y. Optimal specifications for the advanced pedestrian legform impactor. *Stapp Car Crash Journal, 2017, 61:373-395.*
- [12] Isshiki T, Antona-Makoshi J, Konosu A, and Takahashi Y. Simplifying the structural design of the advanced pedestrian legform impactor for use in standardized testing. *SAE Technical Paper, 2018, 01-1049.*
- [13] Isshiki T, Antona-Makoshi J, Konosu A, and Takahashi Y. Consolidated technical specifications for the advanced pedestrian legform impactor (aPLI). *Proceedings of IRCOBI Conference, 2018, Athens, Greece.*
- [14] Gunji Y, Okamoto M and Takahashi Y. Development of a pedestrian pelvis injury index using a human FE model - a further study (in Japanese). *Proceedings of JSAE Spring Conference, 2011, Yokohama, Japan.*
- [15] Akihiko A, Okamoto M and Takahashi Y. Estimation of injury measures for a pedestrian dummy pelvis (in Japanese). *Proceedings of JSAE Spring Conference, 2009, Yokohama, Japan.*
- [16] Edwards K J, Green J F. Analysis of the inter-relationship of pedestrian leg and pelvis. *Proceeding of IRCOBI Conference, 1999, Sitges, Spain.*
- [17] Teresiński G, Madro R. Pelvis and hip joint injuries as a reconstructive factors in car-to-pedestrian accidents. *Forensic Science International, 2001, 124(1):68-73*
- [18] UNECE. JASIC Technical discussion - biofidelity, GTR9-1-05-Rev1e.

APPENDIX A: SPECIFICATIONS OF THREE DIFFERENT SCMs (SEDAN SCM, SUV-LOW SCM, SUV-HIGH SCM)

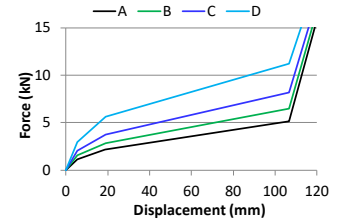
The three different SCMs (Sedan SCM, SUV-Low SCM, SUV-High SCM) were developed based on the specifications of 36 SCMs (18 Low-BP SCMs, 18 High-BP SCMs) which have a wide range of geometric shape and stiffness of sedans and SUVs [10-13]. The Sedan SCM was developed by using the mean value of construction parameters of 18 Low-BP SCMs as shown in Fig. A1 (above). The SUV-Low SCM and SUV- High SCMs were developed by using the mean value of construction parameters of 18 High-BP SCMs except BLE height: 900 mm and 1120 mm respectively, as shown in Fig. A1 (below)

Construction Parameter	Unit	Range			Selected Value	
		18 Low-BP SCMs			Sedan SCM	
		Level 1	Level 2	Level 3		
K1	BLE thickness	mm	0.4	0.6	-	0.5
K2	BP stiffness	-	B	C	D	C
K3	SP stiffness	-	A	C	D	C
H1	BLE height	mm	650	700	750	700
H2	BP height	mm	450	490	530	490
H3	SP height	mm	250	270	350	270
L1	BLE lead	mm	125	200	275	200
L2	SP lead	mm	-20	0	30	0

Definition of dimension (Sedan)



Definition of E



Construction Parameter	Unit	Range			Selected Value		
		18 High-BP SCMs			SUV-Low SCM	SUV-High SCM	
		Level 1	Level 2	Level 3			
K1	BLE thickness	mm	0.4	0.6	-	0.5	0.5
K2	BP stiffness	-	B	C	D	C	C
K3	SP stiffness	-	A	C	D	C	C
H1	BLE height	mm	900	980	1120	900	1120
H4	BP&SP heights difference	mm	40	110	170	110	110
H5	BP&SP avg. height	mm	530	580	670	580	580
L1	BLE lead	mm	110	180	280	180	180
L2	SP lead	mm	0	10	20	10	10

Definition of dimension (SUV)

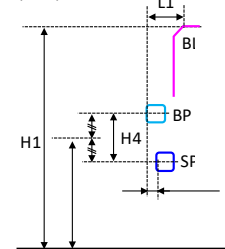
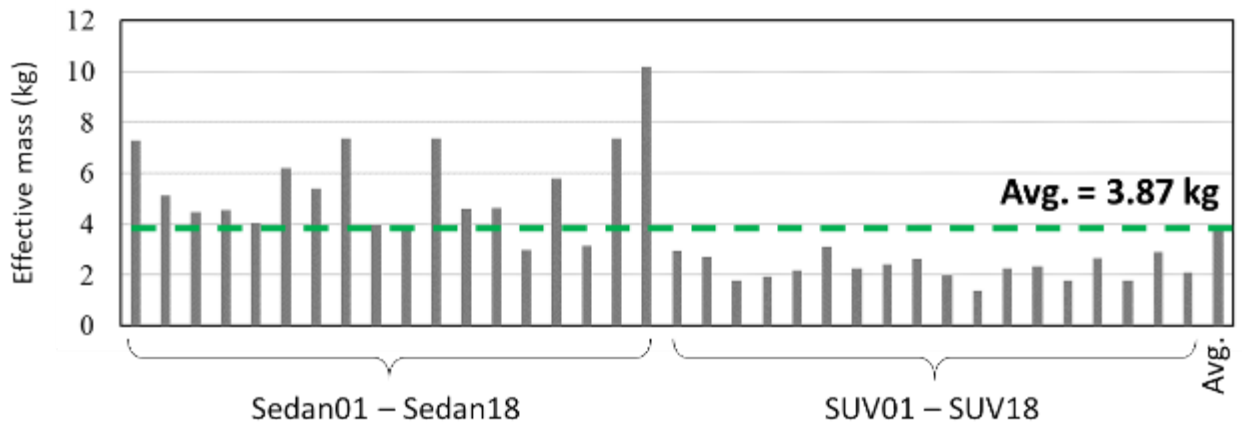


Fig. A1. Specifications of three SCMs (Sedan SCM, SUV-Low SCM, SUV High SCM).

APPENDIX B: EFFECTIVE MASSES OF THE LOWER LIMB ON THE CONTRALATERAL CAR IMPACT SIDE

The effective masses of the lower limb on the contralateral car impact side were calculated using the HBM and 36 SCMs impact simulation results. First, contact force ($F_{ca-SCM\#}$) and acceleration ($a_{ca-SCM\#}$) at the acetabulum on the contralateral car impact side for each SCM were time-integrated from the impact (t_0) to the latest timing of all peak injury measures ($t_{max-SCM\#}$). Second, effective masses ($m_{cl-SCM\#}$) for each SCM were calculated by dividing those values. Averaged effective masses ($m_{cl-avg.}$) were calculated by averaging the $m_{cl-SCM\#}$.



$$m_{cl-avg.} = \frac{1}{36} \sum_{\#=1}^{36} m_{cl-scm\#}$$

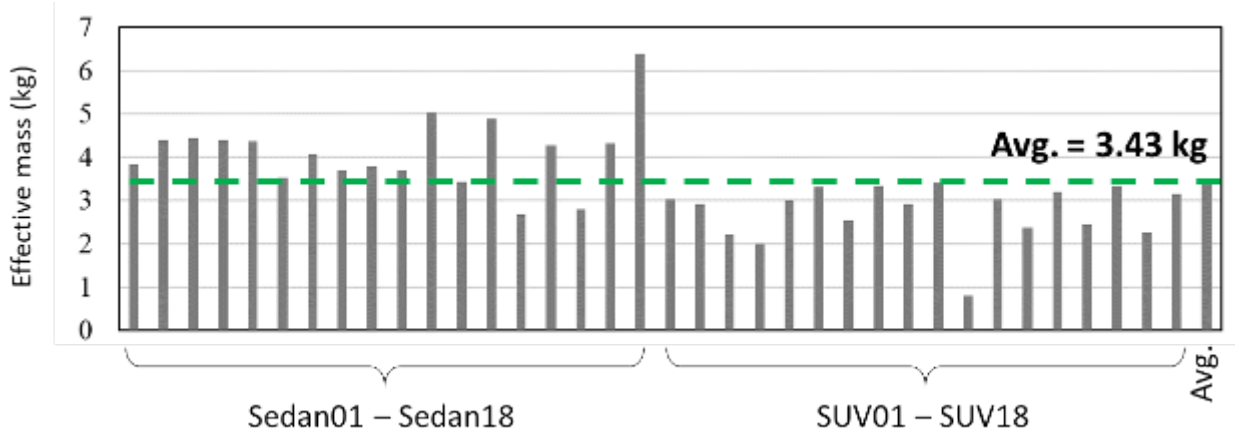
$$m_{cl-scm\#} = \int_{t_0}^{t_{max-scm\#}} F_{ca-scm\#}(t) dt / \int_{t_0}^{t_{max-scm\#}} a_{ca-scm\#}(t) dt$$

- $m_{cl-avg.}$: Averaged effective mass of the lower limb on the contralateral car impact side
- $m_{cl-SCM\#}$: Effective mass of the lower limb on the contralateral car impact side (for each SCM)
- $F_{ca-SCM\#}$: Contact force at the acetabulum on the contralateral car impact side (for each SCM)
- $a_{ca-SCM\#}$: Acceleration at the acetabulum on the contralateral car impact side (for each SCM)
- t_0 : Impact timing
- $t_{max-SCM\#}$: Latest timing of all peak injury measures (for each SCM)

Fig. B1. Effective mass of the lower limb on the contralateral car impact side.

APPENDIX C: EFFECTIVE MASSES OF THE FLESH OF THE HIP ON THE CONTRALATERAL CAR IMPACT SIDE

The effective masses of the flesh of the hip on the contralateral car impact side were calculated using the HBM and 36 SCMs impact simulation results. First, inertial force of the flesh ($F_{cf-SCM\#}$) and acceleration of the ilium ($a_{ci-SCM\#}$) on the contralateral car impact side for each SCM were time-integrated from the impact (t_0) to the latest timing of all peak injury measures ($t_{max-SCM\#}$). Second, effective masses ($m_{cf-SCM\#}$) for each SCM were calculated by dividing those values. Averaged effective masses ($m_{cf-avg.}$) were calculated by averaging the $m_{cf-SCM\#}$.



$$m_{cf-avg.} = \frac{1}{36} \sum_{\# = 1}^{36} m_{cf-scm\#}$$

$$m_{cf-scm\#} = \int_{t_0}^{t_{max-scm\#}} F_{cf-scm\#}(t) dt / \int_{t_0}^{t_{max-scm\#}} a_{cf-scm\#}(t) dt$$

- $m_{cf-avg.}$: Averaged effective mass of the flesh of hip on the contralateral car impact side
- $m_{cf-SCM\#}$: Effective mass of the flesh of hip on the contralateral car impact side (for each SCM)
- $F_{cf-SCM\#}$: Inertial force of flesh of hip on the contralateral car impact side (for each SCM)
- $a_{ci-SCM\#}$: Acceleration at the ilium on the contralateral car impact side (for each SCM)
- t_0 : Impact timing
- $t_{max-SCM\#}$: Latest timing of all peak injury measures (for each SCM)

Fig. C1. Effective mass of the flesh of the hip on the contralateral car impact side.

APPENDIX D: EFFECTIVE MASSES OF THE FLESH OF THE HIP ON THE CONTRALATERAL CAR IMPACT SIDE

F-a1 in Figure 3, the ilium force (struck side), was obtained from contact force between pelvis flesh elements superior to the acetabulum and the SCMs as shown in Figure D1. F-a2 and F-b2 in Figure 3, acetabulum forces (struck side and contralateral side), were measured by means of section forces at the cross sections indicated in Figure D2. F-c in Figure 3, the internal force from the upper body, was obtained by the sum of kinematic joint force and bar element forces representing the ligaments because the upper body and sacrum are connected by the kinematic joint and bar element as shown in Figure D2 (yellow: kinematic joint, red: bar elements). F-b1 in Figure 3, the inertial force from the flesh (contralateral side), cannot be measured by sectional force and/or contact force because the flesh is widely distributed in three dimensions. Therefore, the F-b1 was obtained by the differential of the summational force of the pubic force and the sacroiliac joint force with and without the contralateral side of the flesh as shown in Figure D3.

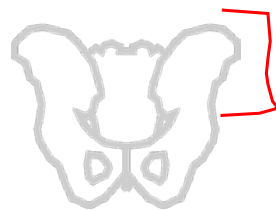


Fig. D1. The area on whose contact force was output to obtain F-a1.

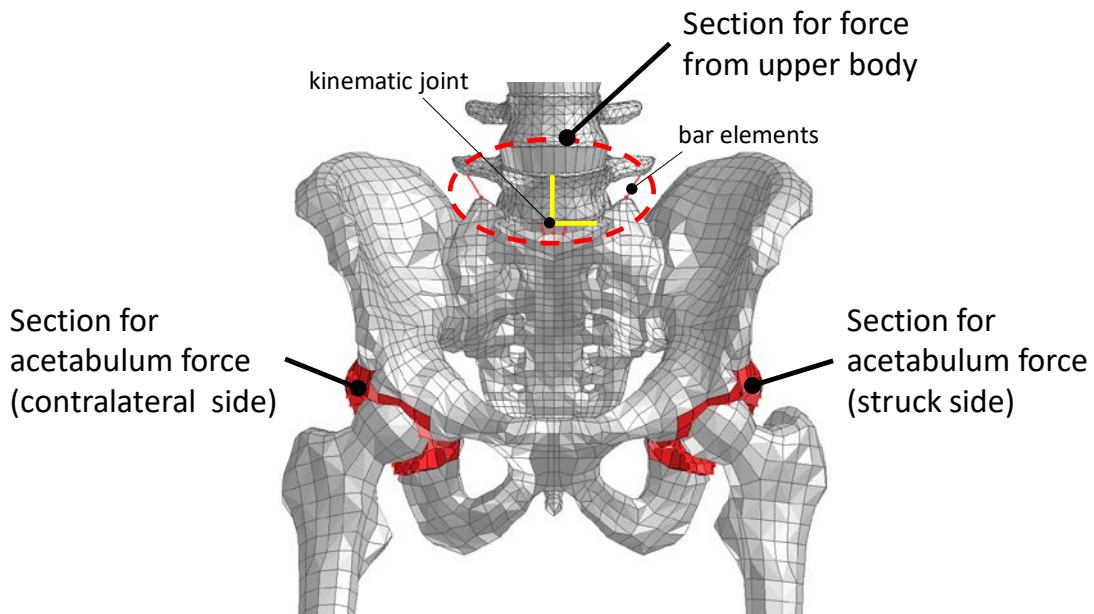
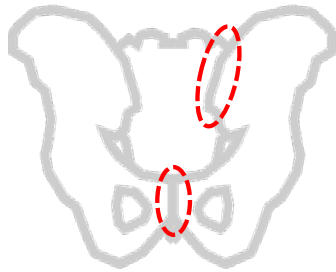


Fig. D1. Sections where F-a2, F-b2 and F-c were measured.

With
contralateral side of flesh



Without
contralateral side of flesh

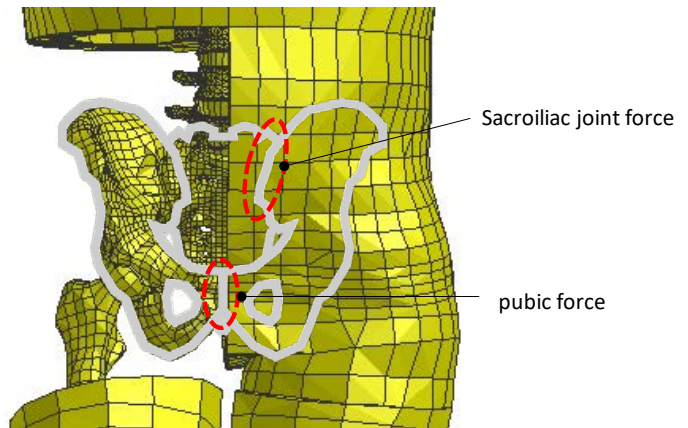


Fig. D3. Differential of summational force of pubic force and sacroiliac force at the condition of with and without contralateral side of flesh were used to calculate F-b1

APPENDIX E: EFFECTIVE MASSES OF THE FLESH OF THE HIP ON THE CONTRALATERAL CAR IMPACT SIDE

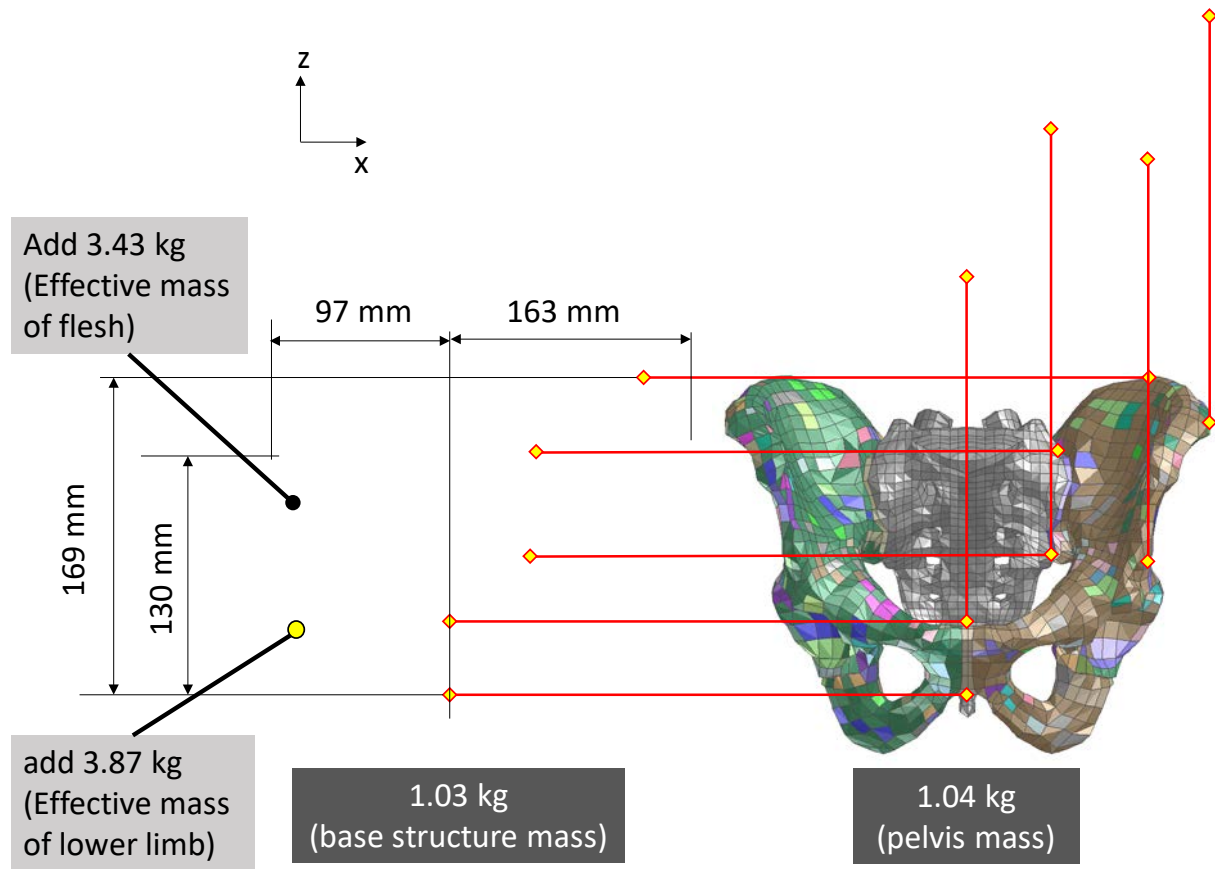


Fig. E1. Mass and geometry of the PPI in contrast with the HBM pelvis.